CHAPTER – 6

Investigation of dielectric and electrochemical behavior of $CaCu_{3-X}Mn_XTi4O12$ (x = 0, 1) ceramic synthesized through semi-wet route

6.1 Introduction

It is very considerable that the giant dielectric constant and low dielectric loss of materials play a vital role in the industrial demand, for the preparation of microelectronic devices such as capacitor-based materials. The $CaCu_3Ti_4O_{12}$ ceramic attracts much attention due to its high dielectric constant at a very low frequency over a wide range of temperature 100 K to 600 K with good thermal stability. It is unfortunate, that the CCTO being the huge dielectric constant, its tangent loss also very high so it is not suitable for practical application in the microelectronic devices.(Adams et al. 2006),(Cai et al. 2007),(D. Mandal et al. 2019),(Berry et al. 2000),(Boonlakhorn and Thongbai 2015a),(Tripathy et al. 2016).The mechanism of the giant dielectric constant of CCTO is till now unreadable. The internal layer barrier capacitance is associated with the insulating grain and grain boundary was proposed by Sinclair group. The novel giant dielectric response mechanism was proposed by Sinclair group which is very acceptable till now. According to this theory, the change in electrical properties of grain and grain boundaries will affect the dielectric properties of materials. The dielectric properties of materials are very sensitive by doping or substitution of ions. For the improvement of giant dielectric properties, most investigation have been focused on the substitution of ions on several cations in the CCTO ceramic to reduce electrical properties of grains and grain boundaries (GBs).(Rani et al. 2018),(Chen et al. 2008) It is well known that enhancement of grain boundaries resistance reduced to low-frequency tan δ value. It was observed from the space charge polarization (or interfacial polarization) that an increase in the mobility of charges inside the semiconducting grain can lead the possibility of gathering of free charges at the interface of insulating layer.(Wu et al. 2011)It is observed from many types of research that doping or substitution successfully at titanium or copper site, improve

particular dielectric properties but almost all the research paper simultaneously degrade other properties. After completing this result there will form give rise to stronger intensity of polarization at internal insulating interfaces resulting increase in dielectric constant. The giant dielectric constant was first reported by Subramanian in $CaCu_3Ti_4O_{12}$ ceramic (Kim et al. 2012).It was observed that many types of research have been available on doping or substitution of ions such as Sr^{+2},La^{+3},Ni^{+2},Mg^{+2},Zn^{+2},Gd^{+3},Sn^{+4},Nb^{+5} in CCTO ceramic have significant value and W^{+6} substitution of many cations Ca^{+2}, Cu^{+2},Ti^{+4} site in the CCTO ceramic have significant value of their dielectric constant (ε') ,tangent loss (δ) and activation electrical conductivity and activation energy at the inside the grain (E_g) and GBs (E_{gb}).(Wu et al. 2011)It is observed from many researches that dopant in titanium or copper site successfully and improve a particular dielectric properties, but almost all the research paper simultaneously degrade (Example to reduce tangent loss δ or enhance ε') other properties. It is mention in many research papers that when higher cations are substituted or dopant at the copper or titanium site due to the presence of excess of electron (*e.g.*, Nb^{5+} or Ta^{5+}) by doping higher cations increase the high dielectric constant (ε') and increase space charge at insulating interfaces .When adding larger cations it is pointed out that decrease in resistance of grain boundaries .It is reported from previous research paper that when small cation doping at CCTO with Mg^{2+} into Cu^{2+} site ,can decrease in tanδ loss and dielectric constant also decrease due decrease in free charges inside the grain boundary .It was observed that Mg^{2+} when doped into Cu^{+2} site ,however the ε' value of Mg-doped CCTO was also decreased due to the decrease in free charges inside the grains, considering by the increase in resistance grain (R_g).(Boonlakhorn and Thongbai 2015b),(Liu et al. 2011)

In this paper, $CaCu_3Ti_4O_{12}$ (CCTO) and $CaCu_2Mn_1Ti_4O_{12}$ (CCMTO) were synthesized by the semi-wet route. Characterization of the CCTO and CCMTO powders obtained

through the Semi-wet route was characterized by X-ray diffraction (XRD), scanning electron microscopy (SEM). Energy Disperse X-ray, Atomic Force Microscopy (AFM), X-ray Photoelectron Spectroscopy After powder sintering process, the pellets were also characterized by dielectric spectroscopy

6.2. Experimental

In this work, $CaCu_3Ti_4O_{12}$ (CCTO) and $CaCu_2Mn_1Ti_4O_{12}$ (CCMTO) were synthesized through the semi-wet route. For the synthesis of both the ceramics ,$Ca(NO_3)_2 \cdot 4H_2O$ (99.2%, Merck, India), copper nitrate, $Cu(NO_3)_2 \cdot 3H_2O$ (99.8%, Merck, India), $Mn(CH_3COO)_2 \cdot 4H_2O$ (99% Merck, India), glycine (99%, Merck, India) and Titanium oxide (oxide TiO_2 99% Merck, India)were taken in the two beaker in the stoichiometric ratio .Glycine was used as a chelating agent. All the metal complexes and glycine were prepared in double-distilled water. The standard molar ratio of both was taken in the two beakers. The solutions were mixed in two beakers of CCTO and CCMTO heated on the hot plate magnetic stirrer, maintaining the temperature 70°C to 80 °C for the evaporation of water until the self-ignition takes place at the room temperature. The process of the same burnt self –propagation which exhausted a large amount of gas and fluffy mass of both CCTO and CCMTO powder. The dry powder which was found, signified as the as-prepared sample. In this method, glycine was used as a chelating agent for metal precursors. It is also found that an organic polyfunctional acid and at least one hydroxyl and carboxylic group as glycine result in the chelation of metal by polycarboxylic acid. In this method , glycine formed the complex with the metal ions at both the amino and carboxylic groups. The glycine plays a vital role in the ignition step. The ignition took very rapidly at a very low temperature due to the presence of glycine. The resultant asp- powder product was ground and calcined using an electrical furnace. The calcined powder then passed into the pellet using a hydraulic

press and providing 4 to 5 ton pressure with the addition of Polyvinyl alcohol (2 wt. %) used as the binder. The pellet of both ceramic burnt out 500°C for two h and finally both ceramic sintered at1100°C for 8 h.

Charactrization

The samples were characterized by X-ray diffraction (XRD) pattern, X-ray Photoelectron Spectroscopy (XPS), Energy Dispersive X-ray spectroscopy (EDS), Scanning Electron Microscopy (SEM), Transition Electron Microscopy (TEM), Atomic Force Microscopy(AFM), Cyclic Voltammetry (CV) and Electrochemical Impedance Spectroscopy (EIS). The microstructure of the fibers were analyzed and correlated with the dielectric and electrical properties.

6.3. Results and discussion

X-ray Diffraction Analysis

Figure 6.1 (a) and (b) display the XRD pattern of CCTO and CCMTO ceramic sintered at 1100°C for 8 h which evidently emphasizes single phase formation of CCTO and CCMTO with body-centered cubic structure. (Kim et al. 2012) All the diffraction peaks of XRD patterns containing the planes (211), (220), (220), (310), (321), (400), (332), (422), (510), (440) pattern confirmed the formation of CCTO and CCMTO ceramic which are correctly justified with the help of JCPDS card No. 75-2188.(Amaral et al. 2010) The existence of minor secondary phase is also observed in CCTO ceramic due to presence of TiO_2 which is confirmed from JCPDS card no. 80-1917. The average crystallite size (D) of both ceramic was calculated by using the Debye Scherer's formula

$$D = \frac{k\lambda}{\beta \cos \theta} (1)$$

In the above equation, where k indicates crystal shape coefficient (k = 0.89), λ is the wavelength (1.54 Å) of the X-ray, β is the full width at half maximum (FWHM) and θ is Braggs diffraction angle. The average crystallite sizes were observed from the Debye Scherer's formula is found to be ~52.39 nm and 38.83 nm for the CCTO and CCMTO ceramic, respectively. It is observed that the average crystalline size decreases with the substitution of Mn in the place of Cu site.

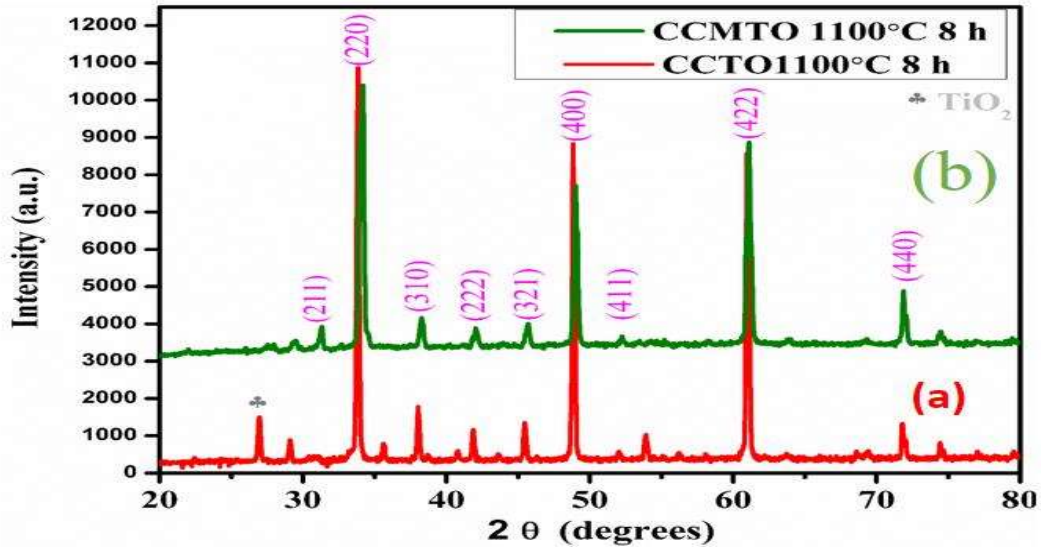

Figure 6.1. XRD patterns of (a) CCTO and (b) CCMTO sintered at 1100 °C for 8 h.

6.3.1. Microstructural studies

High Resolution -Scanning Electron Microscopy (HR – SEM) Studies

Figure 6.2 (a) and (b) display the microstructure of CCTO and CCMTO ceramic, respectively sintered at 1100°C for 8 h. It reveals from fig. that granular formation of grains with polygonal shape is observed in the ceramic which are well separated by the grain boundaries. However, some grains are found spherical in the shape of CCTO and CCMTO ceramic. It is displaying clearly that the grain morphology that the grains observed in CCMTO ceramic are interlocked in a particular fashion to each other as compared to CCTO grain morphology. Any unwanted distortion is not observed in the matrix of synthesized CCTO and CCMTO ceramic. The average grain size of both synthesized materials is calculated with the help of Image J software and found to be 4.63 μm and 7.577 μm, respectively.

Energy Dispersed X-ray (EDX) studies

Figure 6.3 (C) and (d) display the EDX spectrum of CCTO and CCMTO respectively sintered at 1100°C for 8 h. This shows the presence of elemental compositions of calcium, copper, titanium, oxygen and calcium, copper, manganese, titanium, oxygen with their atomic percentage 6.33, 19.01, 24.94, 49.70 and 5.33,17.23,5.30,24.67,47.47, respectively in the synthesized materials The Composition of element of CCTO and CCMTO ceramic supporting by EDX spectrum confirm the purity of the materials.

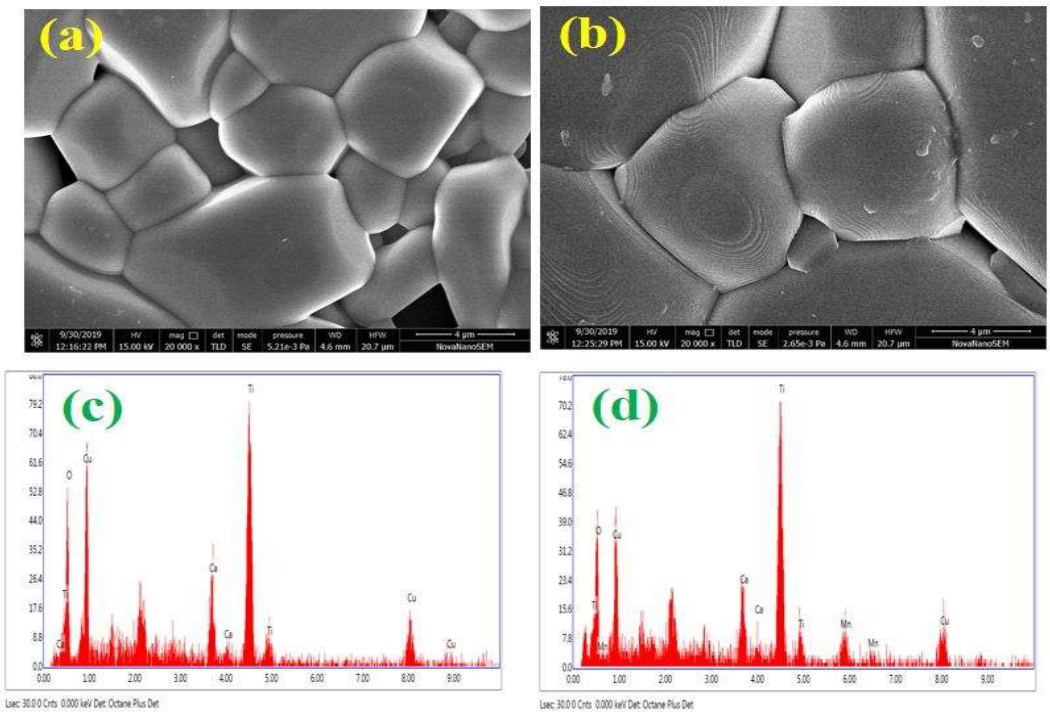

Figure 6.2. SEM micrographs of (a) CCTO and (b) CCMTO sintered at 1100 ℃ for 8 h. EDX spectra of (c) CCTO and (b) CCMTO sintered at 1100 ℃ for 8 h.

Transmission Electron Microscopic Studied (TEM)

Figure 6.3 (a) and (c) display the bright-field TEM image of CCTO and CCMTO ceramic sintered at 1100 ℃ for 8 h, respectively. It is clear from the TEM image that both ceramic consists of polycrystalline particles with cubical shape and dispersion of the particles is also observed in the synthesized materials with some agglomeration. The particle size observed by TEM analysis with the help of Image J software and found to be 120.55 nm and 79.98 nm of CCTO and CCMTO, respectively. Figure 6.3 (b) and (d) displaying the Selected area diffraction (SAED) pattern of both ceramic reveals the presence of a few clear rings in the SEAD pattern also confirmed the polycrystalline nature of the materials.

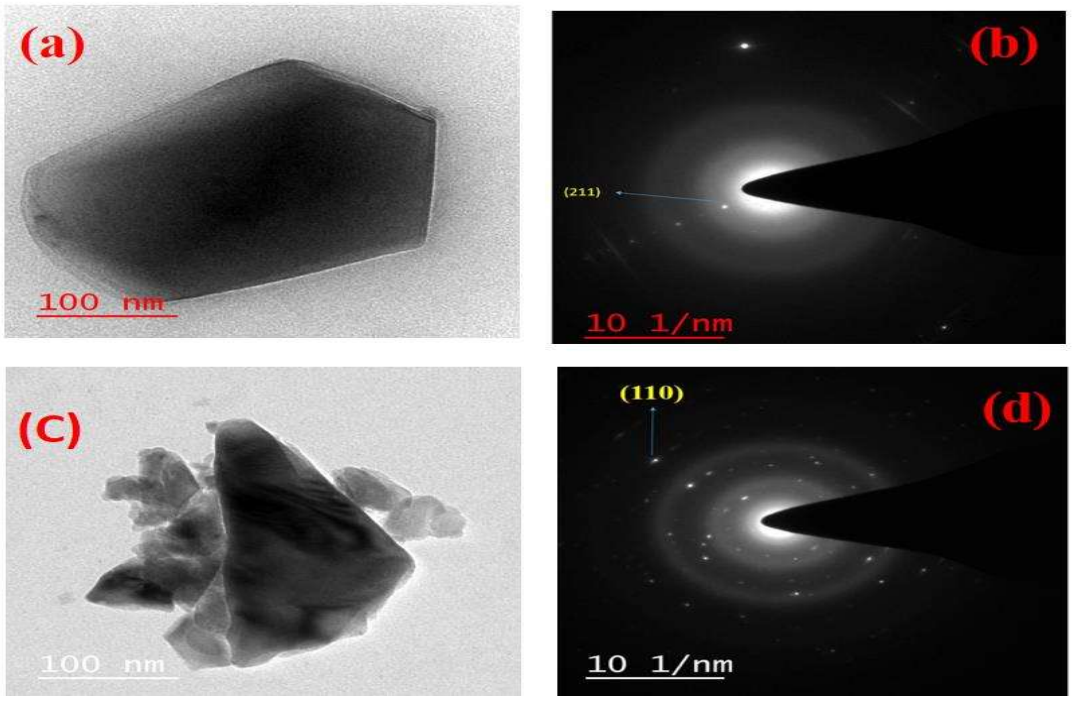

Figure 6.3. HR-TEM images of the $CaCu_3Ti_4O_{12}$ and $CaCu_2Mn_1Ti_4O_{12}$ (a)and (C)at sintered at 1100°C for 8 h and (b) and (d) Indexed SAED patterns of the sintered at 1100 °C for 8 h.

Atomic Force Microscopic (AFM) studies

Figure 6.4 (a),(c) and 6 (a),(c) displays the 2-D AFM image of CCTO and CCMTO ceramic sintered at 1100°C for 8 h, reveals the presence of clear grains separated by grain boundaries with bimodal structure. The three-dimensional image of both CCTO and CCMTO ceramic is shown in figs. 5 (b), and 6 (b). The average roughness (Ra) and root mean squire (RMS) was calculated by using Nova software for 3D image for three-dimensional image and found to be 0.371 µm , 0.431(rms) µm for CCTO ceramic and 0.198 µm, 0.26 (rms) for CCMTO ceramic, respectively. Figure 6.4 (d) and 6.5 (d) show histogram plots for particle size which reveals that most of the roughness of particles was calculated in the range between 30±10 nm of CCTO and CCMTO ceramic.

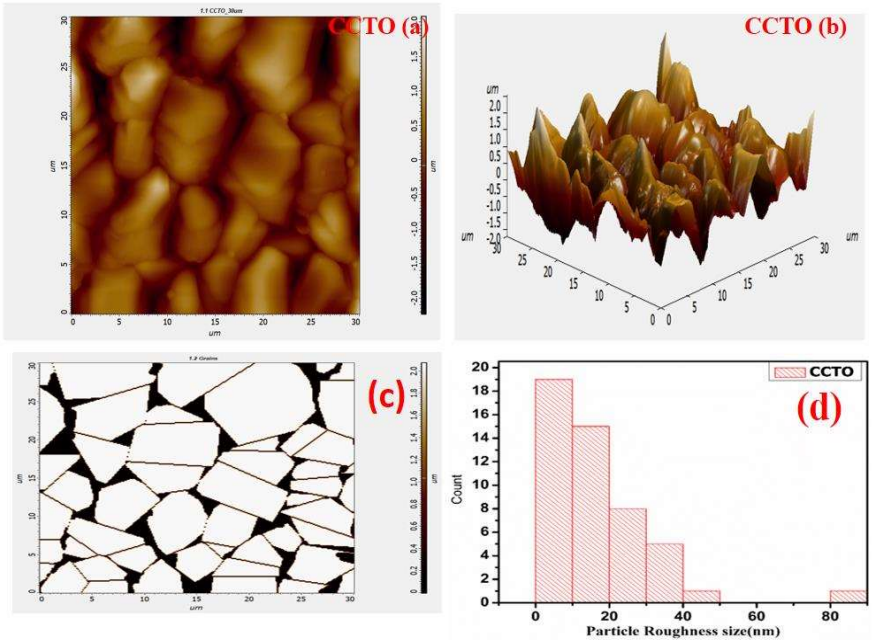

Figure 6.4. (a) and (c) AFM images of CCMTO Ceramic sintered at 1100°C for 8 h two-dimensional image showing grains and grain boundaries (b) Three-dimensional image of surface roughness of CCTO (d) Histogram of three-dimensional particle roughness.

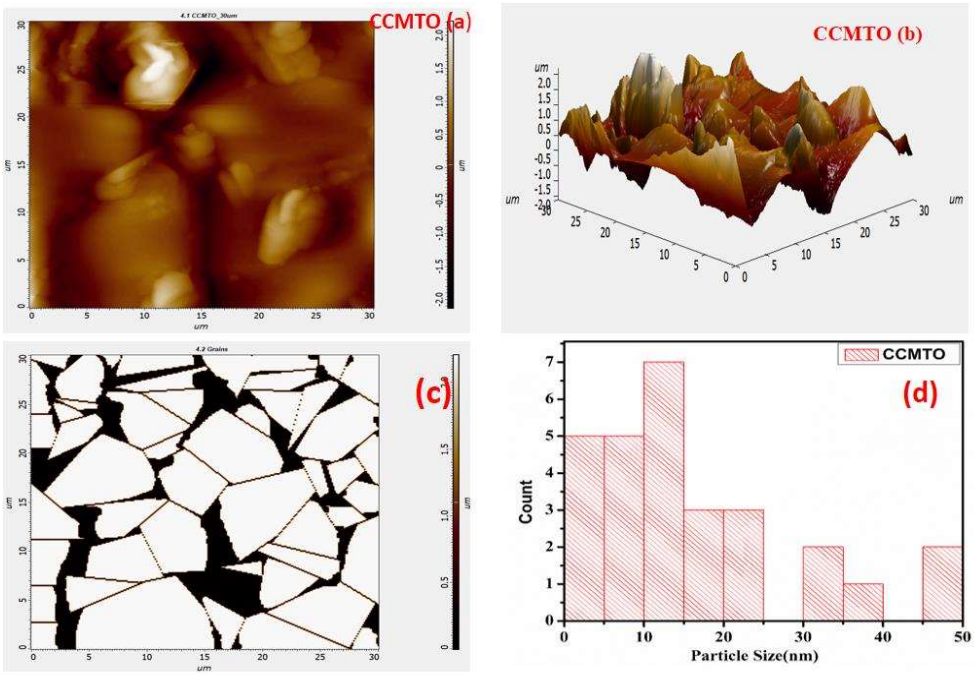

Figure 6.5. (a) and (c) AFM images of CCMTO Ceramic sintered at 1100°C for 8 h two-dimensional image showing grains and grain boundaries (b) Three-dimensional image of surface roughness of CCTO (D) Histogram of three-dimensional particle roughness.

X-ray Photoelectron Spectroscopic (XPS) studies

Figure 6.6 (a) to (d) and (e) to (i) display the XPS spectrum of CCTO and CCMTO, respectively. The XPS measurement has been used for the detection of oxidation of individual elements exist in the materials. In this study, Carbon 1s was taken as reference which has assign value 284.6 eV to compensate surface of charge effects. The presence of metal ions such as, calcium, copper, titanium, oxygen, and manganese in CCTO and CCMTO ceramic with the required oxidation state is investigated by XPS study. The XPS fitting and background subtraction have been performed by using the software XPS-Peak 4.1, which reveals the occurrence of the calcium peak at 347.3 eV and 350.6 eV found in CCMTO ceramic whereas 347.21 eV in CCTO is shown in Fig. 6 (a) and (e). In CCTO $2p_{1/2}$ and in CCMTO two values obtained $^{2}p_{3/2}$ and $^{2}p_{1/2}$ were

found the full-width maxima 1.9 and 2.2.there are very interesting results in both calcium exist in +2 oxidation state in CCTO binding energy was found to be at 347.3 eV $^{2}p_{3/2}$ and in Mn substituted CCMTO binding energy was recorded at 347.3 eV of $Ca^{2}p_{1/2}$, 350 eV $^{2}p_{1/2}$ when Mn substituted intensity ratio in both samples are different. The above results confirm the existence of +2 oxidation state of Ca ion in both ceramic (Jaiswar and Mandal 2017)

Figure 6.6 (b) and (f) display the XPS spectrum of Copper in both of CCTO and CCMTO ceramic and binding energy of copper with satellite peak. The binding energy of copper in CCTO and CCMTO ceramic confirm the existence of +2 oxidation state of Cu with the binding energy related with Cu 2p spectra at the peak 935.8 eV and 954.7 eV that corresponds to Cu $2p_{3/2}$ and Cu $2p_{1/2}$, respectively.(Singh et al. 2014)The XPS spectrum of Mn 2P core level of CCMTO ceramic sintered at 1100°C for 8 h is displayed in Figure 6(h). It is reveals from graph that there are two peaks located at 643.4 eV and 654 eV mainly due to contribution of mixed valent oxidation state of Mn ions corresponds to $Mn^{2}p_{3/2}$ and $Mn^{2}p_{1/2}$ respectively. Furthermore, splitting of these peaks is due to spin-orbital coupling that increases with increasing the temperature-time duration. The convocated peak of Mn 2p region for the CCMTO ceramic sintered at 1100°C for 8 h shown in figure 6.6 (f), which seems to be splitting of Mn 2p into two peaks such as Mn $2p_{3/2}$ and Mn $2p_{1/2}$, respectively. The deconvoluted peaks of Mn $2p_{3/2}$ and Mn 2 $p_{1/2}$ present at 641.4 eV,653.8 eV and 643.8 eV depictthe existence of Mn in variable oxidation states such as Mn^{+2},Mn^{+3} and Mn^{+4}, respectively(Jaiswar and Mandal 2017).

Figure 6.6 (c) and (g) display the XPS spectrum of Titanium of CCTO and CCMTO which shows the two predominant peaks in both ceramic, the positions of peak at 458.1 eV , 464.2 eV of CCTO and 458.2 eV ,467.5 eV of CCMTO which

corresponding to the Ti 2p doublet namely Ti $^2p_{3/2}$ and Ti $^2P_{1/2}$ confirmed the presence of + 4 oxidation state of Ti ion.(Han et al. 2017a) The binding energy peak of Oxygen CCTO and CCMTO ceramic was found to be 529.1 eV, 530.9 eV and 531.1eV, 532.5 eV corresponding to lower and higher binding energy, respectively is shown in Fig 6 (d) and (i). The peak observed at 929.7 eV shows slightly asymmetric type of 1s level.(Jaiswar and Mandal 2017)

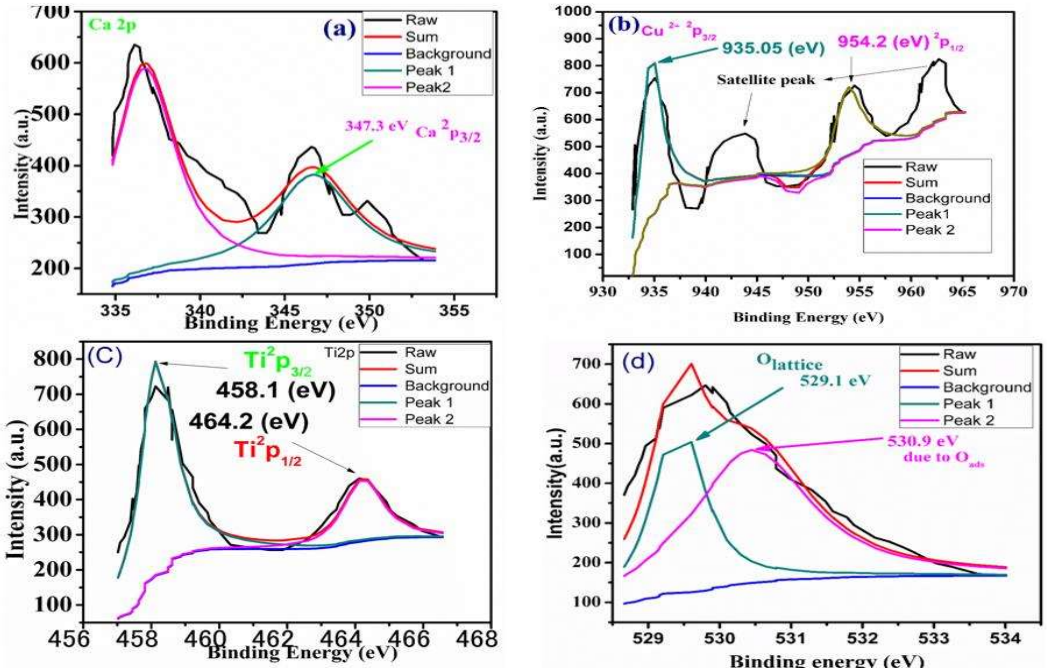

Figure 6.6. (a) to (d) XPS images of the $CaCu_3Ti_4O_{12}$ and at sintered at 1100°C for 8 h .

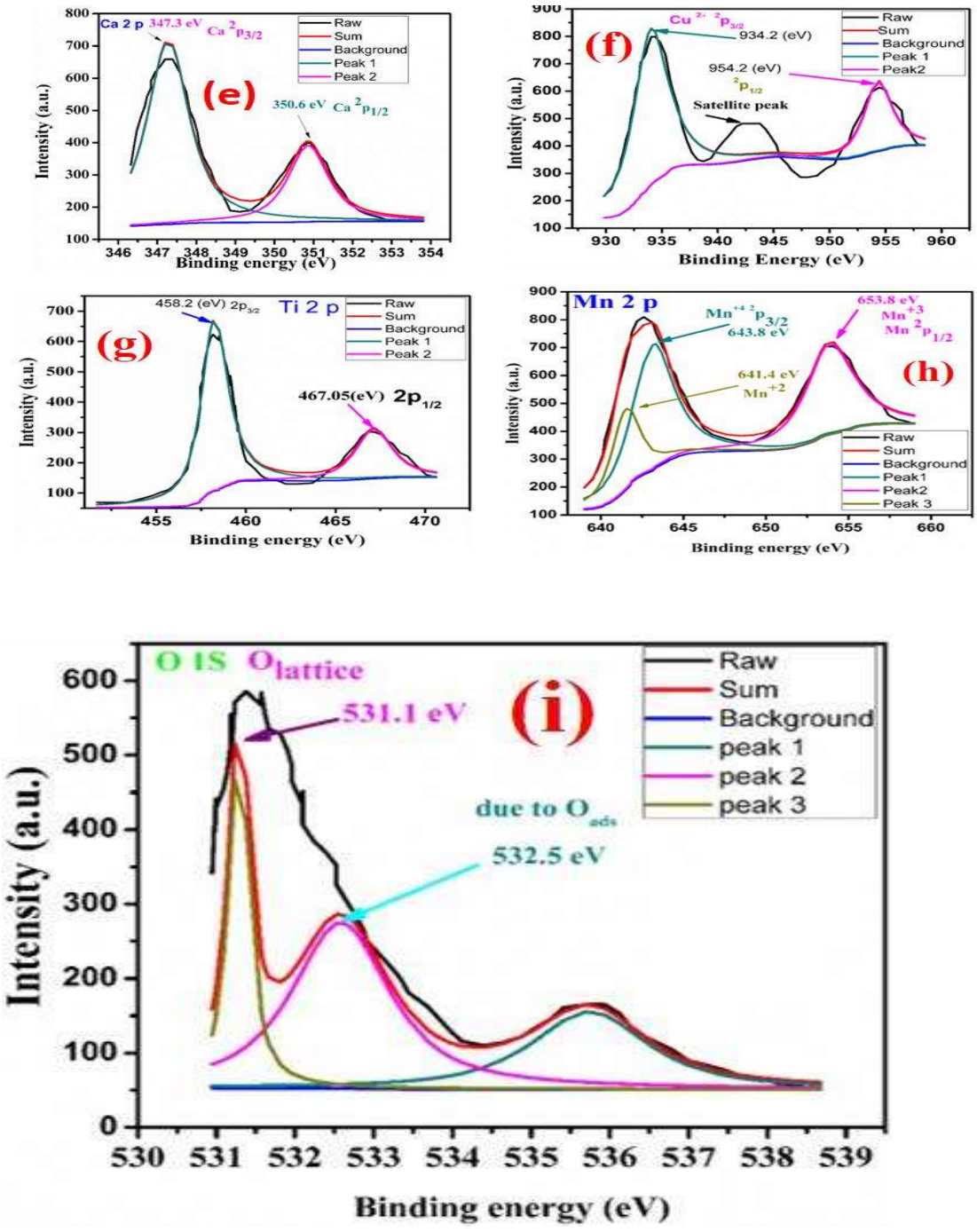

Figure 6.6. (e) to (i) XPS images of the $CaCu_2Mn_1Ti_4O_{12}$ and at sintered at 1100°C for 8 h .

Electrochemical characterization

Fabrication of electrode:-

For the performance of cyclic voltammetry and Electrochemical Impedance Spectroscopy copper wire was taken as the current collector and a substrate (carbon

paper) was devoted to the copper wire with the help of wire insulated by using glue-stick and after that, the dispersion of prepared material (2-propanol of 0.2 mL, Nafion of 12 μL and catalyst) was drop casted on the carbon paper of 1 cm^2 followed by drying for about half an hour in vacuum till complete disappearance of the solvent. The active mass loading was 1 mg/cm^2.

Cyclic voltammetry (CV) and Electrochemical Impedance Spectroscopy (EIS):-

Figure 6.7 (a) and (b) display the cyclic voltammetry (CV) and Electrochemical Impedance Spectroscopy (EIS) of three-electrode system done by versastat 3. In this method, three electrode system of Ag/AgCl, Platinum, and active metal were taken as reference electrode, counter electrode, and the working electrode, respectively.(Das and Verma 2019),(Zinatloo-Ajabshir and Salavati-Niasari 2019),(Zinatloo-Ajabshir et al. 2019a),(Zinatloo-Ajabshir et al. 2019b) Electrochemical Impedance Spectroscopy (EIS) was done at 10 mV amplitude of AC voltage over a frequency range of 100 kHz to 0.01 Hz. For all the electrochemical analysis 1 M KOH electrolyte was taken. Cyclic voltammetry of both the samples were performed at a scan rate of 5 mV/s and a potential window of 1 volt.(Das and Verma 2019) CCMTO exhibits superior electrical conductivity as compared to CCTO, which can be seen from the CV plot. The maximum current generated for CCMTO and CCTO are 3.5 mA and 40 μA, respectively.(Liu et al. 2014),(Zinatloo-Ajabshir et al. 2019d) It is found that the CV results are well supported by EIS results. From the EIS plot, it can be observed that the equivalent series resistance of CCMTO is less than CCTO. This can be recognized to the better contact and wettability of CCMTO in the electrolyte solution.('Electrochemical instability of indium tin oxide (ITO) glass in acidic pH range during cathodic polarization - ScienceDirect' n.d.) The charge transfer resistance of CCMTO and CCTO are 28 ohm and 75 ohm, respectively. The less resistance of

CCMTO is due to the high electronic conductivity and better electrochemical properties of this material. (Das and Verma 2019),(Zinatloo-Ajabshir et al. 2019c),(Zinatloo-Ajabshir et al. 2019f),(Zinatloo-Ajabshir et al. 2019e),

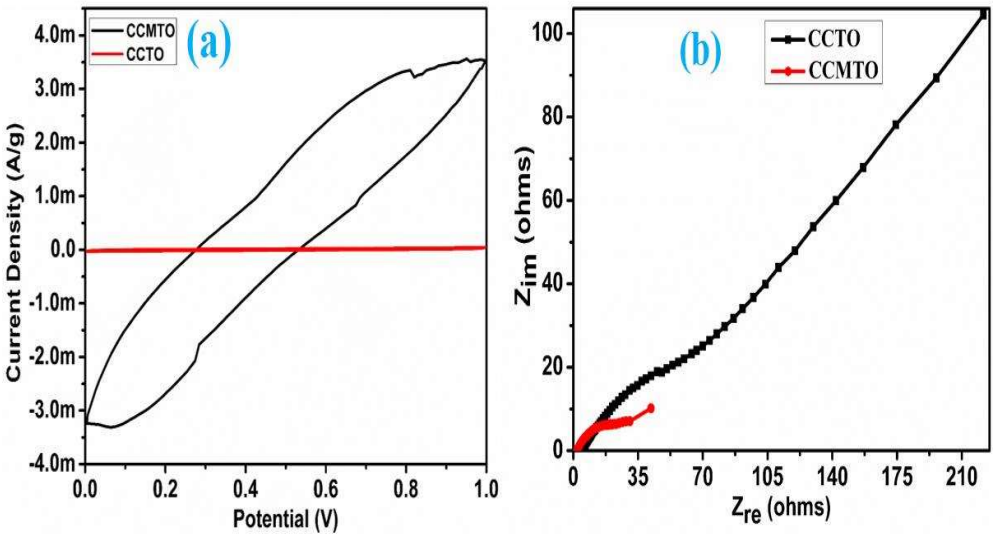

Figure 6.7. (a) displays to cyclic voltammetry and (b) displays Electrochemical Impedance spectroscopy of the $CaCu_2Mn_1Ti_4O_{12}$ and $CaCu_2Mn_1Ti_4O_{12}$ at sintered at 1100°C for 8 h .

6.3.2. Dielectric studies

Figure 6.8 (a), (b) and 9(a), (b) display the variation of temperature and Frequency dependence dielectric constant (ε_r) of CCTO and CCMTO ceramics sintered at 1100°C for 8 h,observed at few selected temperature 313 K,353 K,393 K ,433 K and frequencies 10 Hz, 100Hz,10KHz 100KHz, respectively. The value of dielectric constant exhibits a step like the dielectric constant steeply increases from lower value to higher value in both ceramic CCTO and CCMTO 3×10^3 to $10^4$and 5×10^2 to 3×10^3 respectively. The value of dielectric constant observed predominant at low frequency and reduces at higher frequency region in both ceramic.(Han et al. 2017a),(Amaral et al.

2014),(Sharma et al. 2014),(Kumar et al. 2019),(Supriya et al. 2017) It was observed that at the above room temperature a broad dielectric peak observed in CCTO and CCMTO was found to be 10^4 and 5×10^3 at 10 Hz at few selected frequencies respectively. It is also noted that above the room temperature a broad dielectric peak observed between 313 k to 433 k which is also shift to higher room temperature and decrease in amplitude with increasing higher frequency. It is also clear that a ferroelectric relaxation behavior in both ceramic observed .(Han et al. 2017a),(Kingon et al. 2000),(Boonlakhorn et al. 2014),(Jumpatam et al. 2017).

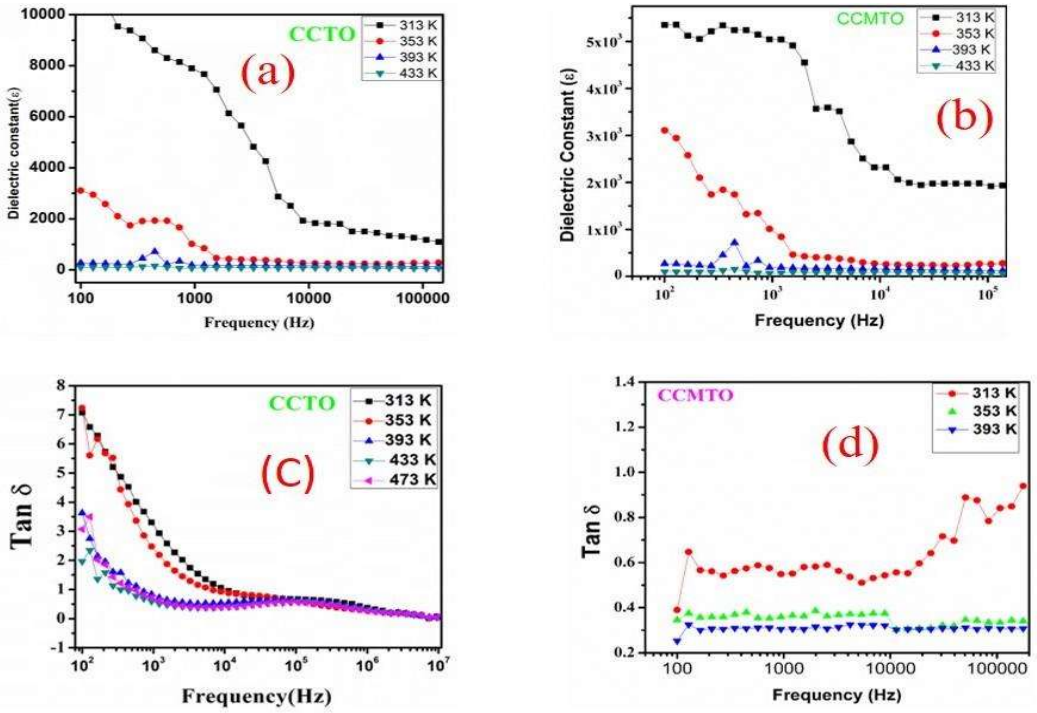

Figure 6.8. (a) and (b) shows the Variations of dielectric constant (ε_r) against frequency at few selected frequency as well as at few selected. (c) and (d) dielectric loss ($\tan\delta$) versus frequency of CCTO ceramic .

Figure 6.8 (c), (d) and 6.9 (c), (d) display the temperature and frequency-dependent tangent loss. It is observed that from the plotted graph , the value of tangent loss of CCTO and in CCMTO7.2and 0.75 ,0.67and 1.6 (temperature(313 K,353K,393 K,433K) respectively and Frequency (10 Hz,100 Hz,10 kHz,100 kHz) the above characteristic behavior of a ferroelectric usually characterized by diffuse the phase transition and strong relaxation dispersion behavior dielectric constant and tangent loss.(Thongbai et al. 2012) It is displaying from the plotted graph tangent loss with a temperature of CCTO and CCMTO ceramic 10 Hz, 100Hz, 10 KHz and 100 KHz ceramic sintered at 1100 °C for 8 h. It is pointed out in both the ceramic at higher frequency temperature-independent whereas temperature dependent at low-frequency region. It is observed that the value of both ceramic at 10 Hz frequency dielectric constant were found to be 10^4(for CCTO) and 5×10^3 (For CCMTO). The region for this result is mainly due to longer sintering process (Sharma et al. 2014),(Amaral et al. 2014) time process more oxygen vacancy in the ceramic and resultant high dielectric constant, displays that the high dielectric constant at 10 Hz was found to be for of both the ceramic 10^4(for CCTO) and 5×10^3 the ceramic at room temperature. The main reason for the high dielectric constant is mainly due to interfacial charge polarization. The origin of interfacial charge polarization arises due to mainly the accumulation of charge carriers at the interface of semiconductor grain and insulating grain boundaries.(Thongbai et al. 2012),(Han et al. 2017b),(A. Molina-García and V. Rees 2016),(Wang et al. 2016)

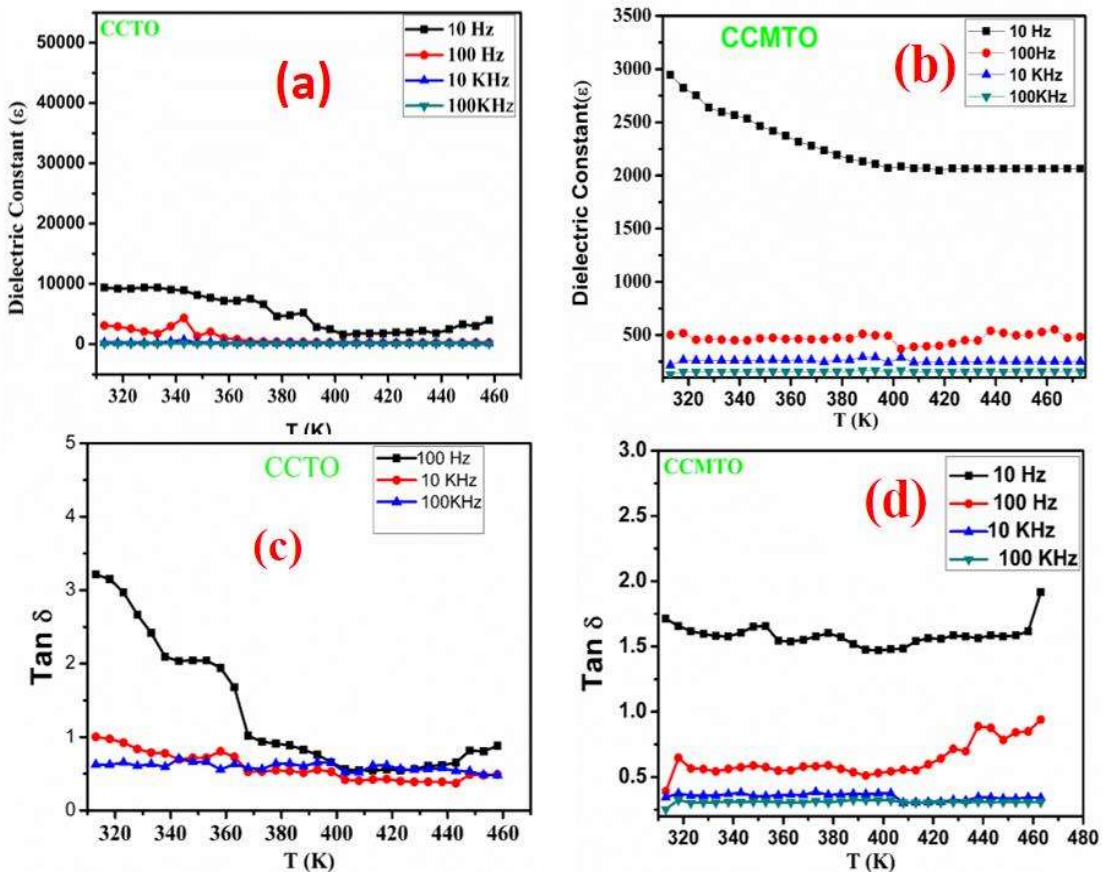

Figure 6.9. (a) and (b) show the variations of dielectric constant (ε_r) against temperature, (c) and (d) dielectric loss (tan δ) versus temperature of CCTO ceramic.

6.3.3. Conclusions

CCTO and CCMTO ceramic were successfully synthesized through a semi-wet route. The phase formation of both the ceramic was confirmed by the XRD pattern. The Microstructure studied were performed by HR-SEM TEM, AFM. The microstructural studies of both the ceramic were observed different grain morphology of CCTO and CCMTO, found 4 μm and around 7.6 μm, respectively. The particle size of CCTO and CCMTO were found to be 120.55 nm and 79.98 nm respectively. The oxidation state was confirmed by XPS. For electrochemical characteristics at operated to both the sample CV and EIS. The maximum current generated for CCMTO and CCTO are 3.5 mA and 40μA respectively. The charge transfer resistance of CCTO and CCMTO are75 ohm and 28 ohm, respectively. It is observed that at low frequency high dielectric constant and at high-frequency low dielectric constant recorded.

References

Adams, T.B., Sinclair, D.C., West, A.R., 2006. Influence of Processing Conditions on the Electrical Properties of CaCu3Ti4O12 Ceramics. *Journal of the American Ceramic Society* **89**, 3129–3135. https://doi.org/10.1111/j.1551-2916.2006.01184.x

Amaral, F., Clemente, E., Valente, M.A., Costa, L., Costa, F., 2014. Effects of Mn doping on the electrical and dielectric properties of CaCu3Ti4O12 fibres. *Ceramics International* **40**, 16503–16511. https://doi.org/10.1016/j.ceramint.2014.08.002

Amaral, F., Valente, M., Costa, L., 2010. Synthesis and Characterization of Calcium Copper Titanate Obtained by Ethylenediaminetetraacetic Acid Gel Combustion. *Materials Chemistry and Physics* **124**, 580–586. https://doi.org/10.1016/j.matchemphys.2010.07.016

A. Molina-García, M., V. Rees, N., 2016. Effect of catalyst carbon supports on the oxygen reduction reaction in alkaline media: a comparative study. *RSC Advances* **6**, 94669–94681. https://doi.org/10.1039/C6RA18894J

Berry, F.J., Greaves, C., Helgason, Ö., McManus, J., Palmer, H.M., Williams, R.T., 2000. Structural and Magnetic Properties of Sn-, Ti-, and Mg-Substituted α-Fe2O3: A Study by Neutron Diffraction and Mössbauer Spectroscopy. *Journal of Solid State Chemistry* **151**, 157–162. https://doi.org/10.1006/jssc.1999.8605

Boonlakhorn, J., Thongbai, P., 2015a. Effect of Annealing in O2 and Mechanisms Contributing to the Overall Loss Tangent of CaCu3Ti4O12 Ceramics. *Journal of Elec Materi* **44**, 3687–3695. https://doi.org/10.1007/s11664-015-3888-0

Boonlakhorn, J., Thongbai, P., 2015b. Mg-doped $CaCu_3Ti_4O_{12}$ nanocrystalline powders prepared by a modified sol–gel method: Preparation, characterization, and their giant dielectric response. *Jpn. J. Appl. Phys.* **54**, 06FJ06. https://doi.org/10.7567/JJAP.54.06FJ06

Boonlakhorn, J., Thongbai, P., Putasaeng, B., Yamwong, T., Maensiri, S., 2014. Very high-performance dielectric properties of Ca1−3x/2YbxCu3Ti4O12 ceramics. *Journal of Alloys and Compounds* **612**, 103–109. https://doi.org/10.1016/j.jallcom.2014.05.143

Cai, J., Lin, Y.-H., Cheng, B., Nan, C.-W., He, J., Wu, Y., Chen, X., 2007. Dielectric and nonlinear electrical behaviors observed in Mn-doped CaCu3Ti4O12 ceramic. *Appl. Phys. Lett.* **91**, 252905. https://doi.org/10.1063/1.2825472

Chen, K., Wu, Y., Liao, J., Liao, J., Zhu, J., 2008. RAMAN AND DIELECTRIC SPECTRA OF CaCu3Ti3.9O12 CERAMICS. *Integrated Ferroelectrics* **97**, 143–150. https://doi.org/10.1080/10584580802089023

D. Mandal, K., Kumar, A., Yadava, S., Singh, Dr.L., Kumar Verma, M., Singh, S., Kumar, V., 2019. Dielectric and electrical properties of zinc doped titanium oxide (TiO2) synthesized by semi-wet route. https://doi.org/10.1117/12.2518203

Das, T., Verma, B., 2019. Polyaniline based ternary composite with enhanced electrochemical properties and its use as supercapacitor electrodes. *Journal of Energy Storage* **26**, 100975. https://doi.org/10.1016/j.est.2019.100975

Electrochemical instability of indium tin oxide (ITO) glass in acidic pH range during cathodic polarization - ScienceDirect [WWW Document], n.d. URL https://www.sciencedirect.com/science/article/pii/S0254058407006396 (accessed 12.24.19).

Han, C.S., Choi, H.R., Choi, H.J., Cho, Y.S., 2017a. Origin of Abnormal Dielectric Behavior and Chemical States in Amorphous $CaCu_3Ti_4O_{12}$ Thin Films on a Flexible Polymer Substrate. *Chem. Mater.* **29**, 5915–5921. https://doi.org/10.1021/acs.chemmater.7b01346

Han, C.S., Choi, H.R., Choi, H.J., Cho, Y.S., 2017b. Origin of Abnormal Dielectric Behavior and Chemical States in Amorphous $CaCu_3Ti_4O_{12}$ Thin Films on a Flexible Polymer Substrate. *Chem. Mater.* **29**, 5915–5921. https://doi.org/10.1021/acs.chemmater.7b01346

Jaiswar, S., Mandal, K.D., 2017. Evidence of Enhanced Oxygen Vacancy Defects Inducing Ferromagnetism in Multiferroic $CaMn_7O_{12}$ Manganite with Sintering Time. *J. Phys. Chem. C* **121**, 19586–19601. https://doi.org/10.1021/acs.jpcc.7b05415

Jumpatam, J., Putasaeng, B., Chanlek, N., Kidkhunthod, P., Thongbai, P., Maensiri, S., Chindaprasirt, P., 2017. Improved giant dielectric properties of $CaCu_3Ti_4O_{12}$ via simultaneously tuning the electrical properties of grains and grain boundaries by F^- substitution. *RSC Adv.* **7**, 4092–4101. https://doi.org/10.1039/C6RA27381E

Kim, C.H., Jang, Y.H., Seo, S.J., Song, C.H., Son, J.Y., Yang, Y.S., Cho, J.H., 2012. Effect of Mn doping on the temperature-dependent anomalous giant dielectric behavior of CaCu 3 Ti 4 O 12. *Phys. Rev. B* **85**, 245210. https://doi.org/10.1103/PhysRevB.85.245210

Kingon, A.I., Maria, J.-P., Streiffer, S.K., 2000. Alternative dielectrics to silicon dioxide for memory and logic devices. *Nature* **406**, 1032–1038. https://doi.org/10.1038/35023243

Kumar, A., Yadava, S.S., Gautam, P., Khare, A., Mandal, K.D., 2019. Magnetic and dielectric studies of barium hexaferrite (BaFe12O19) ceramic synthesized by chemical route. *J Electroceram* **42**, 47–56. https://doi.org/10.1007/s10832-018-0146-x

Liu, Q.X., Tang, X.G., Jiang, Y.P., Dong, F.L., 2011. The Dielectric Characteristics of Sr and Mg Doped CCTO Ceramics [WWW Document]. *Materials Science Forum*. https://doi.org/10.4028/www.scientific.net/MSF.687.416

Liu, X., Fan, H., Shi, J., Dong, G., Li, Q., 2014. High oxide ion conducting solid electrolytes of bismuth and niobium co-substituted La2Mo2O9. *International Journal of Hydrogen Energy* **39**, 17819–17827. https://doi.org/10.1016/j.ijhydene.2014.08.110

Rani, S., Ahlawat, N., Punia, R., Sangwan, K.M., Khandelwal, P., 2018. Dielectric and impedance studies of La and Zn co-doped complex perovskite CaCu3Ti4O12 ceramic. *Ceramics International* **44**, 23125–23136. https://doi.org/10.1016/j.ceramint.2018.09.121

Sharma, S., Yadav, S.S., Singh, M.M., Mandal, K.D., 2014. Impedance spectroscopic and dielectric properties of nanosized $Y_{2/3}$ Cu_3 Ti_4 O_{12} ceramic. *J. Adv. Dielect.* **04**, 1450030. https://doi.org/10.1142/S2010135X14500301

Singh, L., Kim, I.W., Sin, B.C., Mandal, K.D., Rai, U.S., Ullah, A., Chung, H., Lee, Y., 2014. Dielectric studies of a nano-crystalline $CaCu_{2.90}$ $Zn_{0.10}$ Ti_4 O_{12} electro-ceramic by one pot glycine assisted synthesis from inexpensive TiO_2 for energy storage capacitors. *RSC Adv.* **4**, 52770–52784. https://doi.org/10.1039/C4RA08915D

Supriya, D.M., Rajani, M.R., Phani, A.R., Naveen, C.V.S., Ravishankar, R., 2017. Synthesis of CCTO and Doped CCTO Nanopowders and its Applications in the Field of Electronics. *Materials Today: Proceedings*, INTERNATIONAL CONFERENCE ON NANOTECHNOLOGY (ICNANO-2016), APRIL 21-23, 2016, Bangalore, Karnataka **4**, 12021–12025. https://doi.org/10.1016/j.matpr.2017.09.125

Thongbai, P., Jumpatam, J., Putasaeng, B., Yamwong, T., Maensiri, S., 2012. The origin of giant dielectric relaxation and electrical responses of grains and grain boundaries of W-doped $CaCu_3$ Ti_4 O_{12} ceramics. *Journal of Applied Physics* **112**, 114115. https://doi.org/10.1063/1.4768468

Tripathy, N., Das, K.C., Ghosh, S.P., Bose, G., Kar, J.P., 2016. Fabrication of high-k dielectric Calcium Copper Titanate (CCTO) target by solid state route. *IOP Conf. Ser.: Mater. Sci. Eng.* **115**, 012022. https://doi.org/10.1088/1757-899X/115/1/012022

Wang, C., Ni, W., Zhang, D., Sun, X., Wang, J., Li, H., Zhang, N., 2016. Dielectric properties of pure and Mn-doped CaCu3Ti4O12 ceramics over a wide temperature range. *J Electroceram* **36**, 46–57. https://doi.org/10.1007/s10832-016-0024-3

Wu, Y.J., Su, S.H., Wu, S.Y., Chen, X.M., 2011. Microstructures and dielectric properties of spark plasma sintered Ba0.4Sr0.6TiO3/CaCu3Ti4O12 composite ceramics. *Ceramics International* **37**, 1979–1983. https://doi.org/10.1016/j.ceramint.2011.02.006

Zinatloo-Ajabshir, S., Morassaei, M.S., Salavati-Niasari, M., 2019a. Eco-friendly synthesis of Nd2Sn2O7–based nanostructure materials using grape juice as green fuel as photocatalyst for the degradation of erythrosine. *Composites Part B: Engineering* **167**, 643–653. https://doi.org/10.1016/j.compositesb.2019.03.045

Zinatloo-Ajabshir, S., Morassaei, M.S., Salavati-Niasari, M., 2019b. Facile synthesis of Nd2Sn2O7-SnO2 nanostructures by novel and environment-friendly approach for the photodegradation and removal of organic pollutants in water. *Journal of Environmental Management* **233**, 107–119. https://doi.org/10.1016/j.jenvman.2018.12.011

Zinatloo-Ajabshir, S., Morassaei, M.S., Salavati-Niasari, M., 2019c. Simple approach for the synthesis of Dy2Sn2O7 nanostructures as a hydrogen storage material from banana juice. *Journal of Cleaner Production* **222**, 103–110. https://doi.org/10.1016/j.jclepro.2019.03.023

Zinatloo-Ajabshir, S., Salavati-Niasari, M., 2019. Preparation of magnetically retrievable CoFe2O4@SiO2@Dy2Ce2O7 nanocomposites as novel photocatalyst for highly efficient degradation of organic contaminants. *Composites Part B: Engineering* **174**, 106930. https://doi.org/10.1016/j.compositesb.2019.106930

Zinatloo-Ajabshir, S., Salehi, Z., Amiri, O., Salavati-Niasari, M., 2019d. Green synthesis, characterization and investigation of the electrochemical hydrogen storage properties of Dy2Ce2O7 nanostructures with fig extract. *International Journal of Hydrogen Energy* **44**, 20110–20120. https://doi.org/10.1016/j.ijhydene.2019.05.137

Zinatloo-Ajabshir, S., Salehi, Z., Amiri, O., Salavati-Niasari, M., 2019e. Simple fabrication of Pr2Ce2O7 nanostructures via a new and eco-friendly route; a potential electrochemical hydrogen storage material. *Journal of Alloys and Compounds* **791**, 792–799. https://doi.org/10.1016/j.jallcom.2019.04.005

Zinatloo-Ajabshir, S., Salehi, Z., Salavati-Niasari, M., 2019f. Synthesis of dysprosium cerate nanostructures using Phoenix dactylifera extract as novel green fuel and investigation of their electrochemical hydrogen storage and Coulombic efficiency. *Journal of Cleaner Production* **215**, 480–487. https://doi.org/10.1016/j.jclepro.2019.01.026